Medicinal Chemistry Research (2019) 28:143–159
https://doi.org/10.1007/s00044-018-2272-z

MEDICINAL CHEMISTRY RESEARCH

ORIGINAL RESEARCH

Comparative α-glucosidase and α-amylase inhibition studies of rhodanine–pyrazole conjugates and their simple rhodanine analogues

Parvesh Singh[1] · Serisha Mothilal[1] · Nagaraju Kerru[1] · Ashona Singh-Pillay[1] · Lalitha Gummidi[1] · Ochuko L. Erukainure[2] · Md. Shahidul Islam[2]

Received: 10 August 2018 / Accepted: 4 December 2018 / Published online: 13 December 2018

Abstract

Novel rhodanine–pyrazole conjugates (**6a–i**) and their simple rhodanine analogues (**8a–e**) were prepared and comparatively screened for their antidiabetic activities against enzymatic targets, α-glucosidase and α-amylase. As expected, the molecular hybrids exhibited significantly greater inhibitory activity against α-glucosidase ($IC_{50} = 2.259 \times 10^{-6}$–$1.160 \times 10^{-4}$ mol/L), relative to their simple rhodanine counterparts ($IC_{50} = 3.056 \times 10^{-4}$–$9.494 \times 10^{-4}$ mol/L). Amongst the screened derivatives compounds **6a** and **6f** displayed a 3-fold and 42-fold greater potency against α-glucosidase ($IC_{50} = 2.854 \times 10^{-5}$ and 2.259×10^{-6}mol/L, respectively) compared to the standard drug, acarbose. The designed molecular conjugates displayed an improved binding affinity toward α-glucosidase than α-amylase. Compound **6d** was identified as the most potent inhibitor of α-amylase ($IC_{50} = 6.377 \times 10^{-5}$ mol/L) with a 1.5-fold greater inhibitory activity than acarbose. Structural assessment of the molecules revealed that electron withdrawing (Cl) and electron donating (OCH_3) groups at the *ortho*-position played a significant role in the inhibitory activity. Molecular docking studies of the molecular conjugates and simple rhodanine analogues in the active site of α-glucosidase were performed to describe and highlight the putative binding interactions attributing to the selective inhibition. The identification of these novel rhodanine–pyrazole molecular hybrids forms part of a potential treatment in the management of diabetes.

Keywords Pyrazole · Rhodanine · Molecular hybrids · α-glucosidase · α-amylase

Introduction

Type II diabetes is a chronic disease which has largely been characterised by poor lifestyle choices (Browlee 2001; Sundarram and Murthy 2014; Sales et al. 2012; Taha et al. 2017). It is a serious disease that when untreated or mismanaged has been associated with severe complications, such as cardiovascular, retinopathic and neuropathic diseases.

Current therapies in the management of diabetes include oral administration of antidiabetic drugs, intramuscular insulin injection, as well as dietary (e.g. low glycemic index foods) and lifestyle changes (Kaku 2014; Mata et al. 2013). However, these techniques have limited efficacy and suffer a number of limitations; hence the need to find new and innovative antidiabetic therapies. Two of the most attractive targets of antidiabetic chemotherapeutics in the control of blood glucose levels are α-glucosidase and α-amylase enzymes.

α-Glucosidase and α-amylase are key enzymes that degrade carbohydrates into sugars (Fig. 1). The α-glucosidase enzyme is responsible for hydrolysing polysaccharides into glucose at the terminal non-reducing α-1-4-glycosidic bond in the small intestine (Taha et al. 2015). Over-expression of the enzyme can lead to increased levels of

Supplementary information The online version of this article (https://doi.org/10.1007/s00044-018-2272-z) contains supplementary material, which is available to authorized users.

✉ Parvesh Singh
parveshdurban@gmail.com
singhp4@ukzn.ac.za

[1] School of Chemistry and Physics, University of KwaZulu-Natal, P/Bag X54001, Westville, Durban 4000, South Africa

[2] Biomedical Research Lab, Department of Biochemistry, School of Life Sciences, University of KwaZulu-Natal, Westville Campus, Durban 4000, South Africa

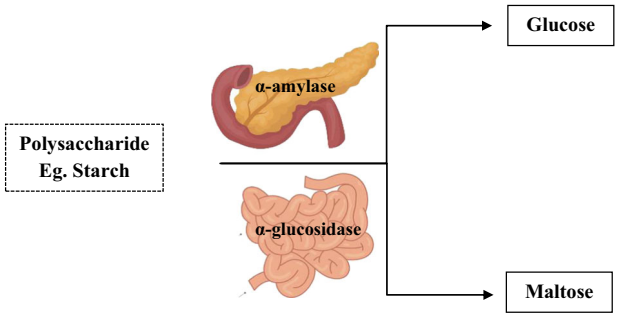

Fig. 1 Antidiabetic metabolic targets

glucose in the blood. α-Amylase works in a similar way and is found in the pancreas and saliva. It hydrolyses the α-bond of large α-linked polysaccharides, such as starch and glycogen, to glucose and maltose (Kazeem et al. 2013). Thus, the inhibition of the α-glucosidase and α-amylase enzymes is essential for delaying carbohydrate degradation and glucose absorption, which decreases the amount of overall glucose in the body, and inevitably reduces the effect of diabetes (Kazeem et al. 2013).

Current α-glucosidase and α-amylase inhibitors, such as acarbose, voglibose and miglitol, are stable in the gastrointestinal tract and have found clinical application as antidiabetic drugs (Moorthy et al. 2012; Shahidpour et al. 2015). However, they are also allied with various undesirable side effects such as diarrhoea, abdominal pain and flatulence, which leads to some patients discontinuing therapy. Unfortunately, the various side-effects associated with the existing α-glucosidase and α-amylase inhibitor reiterate the need for the development of new therapies, in the form of potent antidiabetic drugs with no or low-risk side effects.

In this study, a molecular hybrid approach is employed which combines the biologically active scaffolds of pyrazole, rhodanine and a dinitro-aromatic (Fig. 2), each with its novel mechanism of action as potential antidiabetic agents specifically targeting α-glucosidase and α-amylase enzymes (Kashtoh et al. 2016; Chaudhry et al. 2018). Pyrazole derivatives have proven to have significant metabolic stability and pharmacological efficiency as antidiabetic agents (Viseras et al. 2014; Vazquez et al. 2017). Teneligliptin is an oral DPP-4 inhibitor containing pyrazole, and was approved for the treatment of type-II diabetes (Sharma et al. 2016).

Rhodanine forms an important class of heterocyclic compounds, which have gained increased attention in medicinal chemistry and drug discovery over the past few years (Werner et al. 2015; Ramesh et al. 2014; Reddy et al. 2014). However, in recent years, there has been an increased interest in exploiting rhodanine-based compounds for their antidiabetic activity (Murugan et al. 2009; Agrawal et al. 2015). An example of this is the drug Epalrestat, an aldose reductase inhibitor which is clinically used for the treatment of diabetic neuropathy (Terashima et al. 1984). In a recent study, Andleeb et al. (2016) reported the synthesis of a series of pyrazole–rhodanine conjugates (compound E, $IC_{50} = 1.22\ \mu M$) that showed potent aldose reductase inhibitory activity.

Nitro-aromatic compounds have demonstrated extensive target selectivity and are reported to be pharmacologically active and robust (Patterson and Wyllie 2014; Ju and Parales 2010; Hall et al. 2011; Hall and Wilkinson 2012). For example, 2-nitrobenzimidazole has been reported to possess comparable activity to glibenclamide (an antidiabetic drug) in alloxan-induced diabetic rats (Bathini et al. 2013). Amongst different synthetic approaches being used in drug discovery, molecular hybridization (MH) is gaining popularity due to its ability to combine two or more biologically active scaffolds with a different or novel mechanism of action (Berube 2016; Kerru et al. 2017a; Singh et al. 2017). This supports our research rationale, in combining the pharmacophore nuclei of pyrazole, rhodanine and nitroaromatic into a single architecture. It was also envisaged that the structural variations to the 3-phenyl ring of pyrazole, as well as substituting the acetyl moiety at the N3-position of the rhodanine may reveal a more potent antidiabetic inhibitor.

Accordingly, in continuation of our interest (Singh et al. 2018; Kerru et al. 2017b) a novel series of rhodanine–pyrazole conjugates (**6a–i**) and their simple rhodanine analogues (**8a–e**) was developed, and evaluated in vitro against α-glucosidase and α-amylase enzymes. Furthermore, the structure assessment and molecular docking studies of these compounds were also performed to describe the critical pharmacophoric features contributing to inhibitory activity.

Materials and methods

Chemistry

All chemicals (laboratory grade) and solvents used in this study were purchased from Sigma Aldrich and Merck, and used as such without any further purification. Dimethylformamide (DMF) was dried for 12 h using molecular sieves 3 Å, which were regenerated by preheating at 250 °C. The progress of reactions and the purity of the compounds were determined using aluminium backed TLC plates (Kieselgel 60 F254 plates), purchased from Merck. The spots were visualized using 254 nm wavelength ultraviolet light. The nuclear magnetic resonance (NMR) analysis was recorded on a Bruker AVANCE III 400 MHz spectrometer (399.995 MHz for ^{1}H and 100.4296 MHz for ^{13}C). Chemical shifts (δ) were reported in parts per million (ppm). The

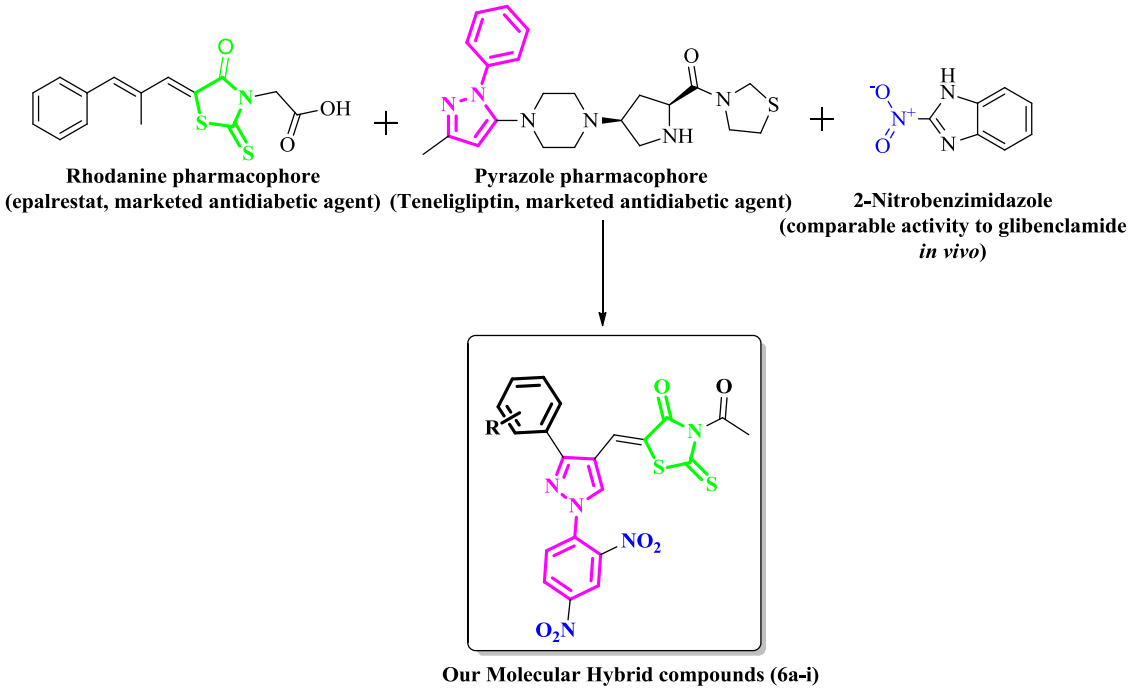

Fig. 2 Design of the molecular conjugates (**6a–i**) as antidiabetic agents

solvent used for NMR analysis was deuterated dimethyl sulfoxide-d_6. The chemical shifts for ^{1}H and ^{13}C are referenced to DMSO-d_6 at 2.50 ppm and 39.51 ppm, respectively. The 2D NMR experiments such as HSQC, HMBC, COSY and NOESY were conducted with 4 K × 128 data points (t2 × t1). The spin multiplicities are abbreviated as follows: singlet (s), doublet (d), doublet of doublets (dd), triplet (t) and multiplet (m). The NMR data was analysed using TopSpin 3.1 software (Bruker). Melting points of compounds were determined in an electro thermal melting point apparatus (Electro Thermal IA9100) using sealed capillary tubes, and are uncorrected. Infrared spectra were recorded on a Perkin Elmer Spectrum 100 FTIR spectrometer with universal ATR sampling accessory. High-resolution mass data were obtained for synthesized compounds using a Bruker Micro ESI-QTOF instrument, which is operated at ambient temperatures. The concentration of each sample used in HRMS analysis was approximately 1 ppm. Absorbance readings done for the antidiabetic testing was obtained using a Synergy/HTX multi-mode reader by BioTek. The absorbance wavelengths for each enzyme are specified in the relevant section.

General procedure for the synthesis of substituted (E)-1-(2,4-dinitrophenyl)-2-(1-phenyl etylidene) hydrazines (3a–i)

A mixture of acetophenone (**1a–i**) (0.01 mol) and 2,4-dinitrophenyl hydrazine (**2**) (0.02 mol), dissolved in ethanol (10 mL), was added dropwise to sulfuric acid (1.0 mL) while stirring. The reaction mixture was further stirred for 1 h at room temperature and then cooled in ice bath to complete the crystallization. The solid was filtered under suction with the aid of ethanol.

General procedure for the synthesis of substituted 1-(2,4-dinitrophenyl)-3-phenyl-1H-pyrazole-4-carbaldehydes (4a–i)

To a solution of DMF (6 mL) and $POCl_3$ (0.5 g, 3.0 mmol), 1-phenyletylidene hydrazines (1.0 mmol) (**3a–i**) was added and the reaction was allowed to stir at 60 °C for 5 h. The resulting mixture was poured into ice cold water, neutralized using a saturated solution of sodium hydroxide, and the solid product was filtered, washed with water, dried and recrystallized from ethanol.

General procedure for the synthesis of pyrazole–rhodanine derivatives (6a–i)

Substituted pyrazole-4-carbaldehydes (**4a–i**) (0.01 mmol), rhodanine (**5**) (0.012 mmol) and anhydrous sodium acetate (0.03 mmol) were dissolved in 15 mL of acetic acid and refluxed for 3 h. Once the completion of the reaction was confirmed by TLC, solvent was removed using a high vacuum. The reaction mixture was then poured on crushed ice and the obtained solid was filtered and purified using column chromatography.

(Z)-3-Acetyl-5-((1-(2,4-dinitrophenyl)-3-phenyl-1H-pyrazol-4-yl)methylene)-2-thioxo thiazolidin-4-one (6a)

Orange solid; Yield: 59%; mp 139–140 °C; FTIR ν_{max} (cm^{-1}): 3085.92 (C–H), 1703.46 (C=O), 1529.53 (NO_2), 1174.34 (C=S), 1059.04 (C–N); ^{1}H NMR (400 MHz, DMSO-d_6): δ_H 4.26 (s, 3H, CH_3), 6.98 (s, 1H, $CH_{olefinic}$), 7.50–7.70 (m, 5H, ArH), 8.41 (d, J_{HH} = 8.92 Hz, 1H, ArH), 8.68–8.71 (dd, J_{HH} = 2.52, 8.92 Hz, 1H, ArH), 8.91 (d, J_{HH} = 2.36 Hz, 1H, ArH), 8.98 (s, 1 H, $CH_{pyrazole}$); ^{13}C NMR (100 MHz, DMSO-d_6): δ_C 29.71, 119.72, 121.21, 122.86, 123.33, 126.57, 128.18, 128.57, 128.64, 129.62, 130.30, 135.03, 138.67, 143.01, 146.37, 153.84, 166.45, 176.65, 184.65; HRMS *m/z* (pos): 518.0590 $C_{21}H_{13}N_5O_6S_2Na$ (calcd: 518.0591).

(Z)-3-Acetyl-5-((3-(2-chlorophenyl)-1-(2,4-dinitrophenyl)-1H-pyrazol-4-yl)methylene)-2-thioxothiazolidin-4-one (6b)

Yellow solid; Yield: 78%; mp 190–192 °C; FTIR ν_{max} (cm^{-1}): 3064.49 (C–H), 1700.31 (C=O), 1529.56 (NO_2), 1172.16 (C=S), 1067.08 (C–N); ^{1}H NMR (400 MHz, DMSO-d_6): δ_H 4.26 (s, 3H, CH_3), 7.37 (s, 1H, $CH_{olefinic}$), 7.54–7.57 (m, 4H, ArH), 8.40 (d, J_{HH} = 8.88 Hz, 1H, ArH), 8.67–8.87 (dd, J_{HH} = 2.44, 8.88 Hz, 1H, ArH), 8.91 (d, J_{HH} = 2.44 Hz, 1H, ArH), 8.92 (s, 1H, $CH_{pyrazole}$); ^{13}C NMR (100 MHz, DMSO-d_6): δ_C 31.32, 116.73, 120.45, 121.15, 126.30, 126.90, 127.96, 128.57, 128.74, 128.93, 129.11, 129.56, 130.24, 132.09, 135.14, 142.83, 146.11, 155.07, 168.91, 176.64, 194.93; HRMS *m/z* (pos): 551.9636 $C_{21}H_{12}N_5O_6S_2ClNa$ (calcd: 551.9644).

(Z)-3-Acetyl-5-((1-(2,4-dinitrophenyl)-3-(4-fluorophenyl)-1H-pyrazol-4-yl)methylene)-2-thioxothiazolidin-4-one (6c)

Orange solid; Yield: 74%; mp 142.0–145.8 °C; FTIR ν_{max} (cm^{-1}): 3075.65 (C–H), 1704.53 (C=O), 1541.72 (NO_2), 1184.29 (C=S), 1080.83 (C–N); ^{1}H NMR (400 MHz, DMSO-d_6): 4.25 (s, 3H, CH_3), 7.34 (s, 1H, $CH_{olefinic}$), 7.44 (t, J_{HH} = 8.72, Hz, 2 H, ArH), 7.58–7.62 (dd, J_{HH} = 5.8, 8.72, Hz, 2H, ArH), 8.39 (d, J_{HH} = 8.88 Hz, 1H, ArH), 8.62 (d, J_{HH} = 7.48 Hz, 1H, ArH), 8.67–8.69 (dd, J_{HH} = 2.04, 8.88 Hz, 1H, ArH), 8.92 (s, 1H, $CH_{pyrazole}$); ^{13}C NMR (100 MHz, DMSO-d_6): δ_C 31.32, 107.11, 115.75, 116.11, 116.33, 116.72, 120.33, 121.16, 124.57, 126.45, 126.74, 126.94, 127.72, 127.99, 130.74, 130.82, 132.16, 135.10, 142.82, 145.01, 146.13, 154.08, 168.86, 176.64, 194.90; HRMS *m/z* (pos): 536.0775 $C_{21}H_{12}N_5O_6S_2FNa$ (calcd: 536.0770).

(Z)-3-Acetyl-5-((1-(2,4-dinitrophenyl)-3-(4-hydroxyphenyl)-1H-pyrazol-4-yl)methylene)-2-thioxothiazolidin-4-one (6d)

Orange solid; Yield: 65%; mp 146–147 °C; FTIR ν_{max} (cm^{-1}): 3405.96 (O–H), 3096.04 (C–H), 1704.81 (C=O), 1512.08 (NO_2), 1174.07 (C=S), 1083.10 (C–N); ^{1}H NMR (400 MHz, DMSO-d_6): δ_H 4.26 (s, 3H, CH_3), 6.84 (d, J_{HH} = 8.44 Hz, 2H, ArH), 7.05 (s, 1H, $CH_{olefinic}$), 7.63 (d, J_{HH} = 8.44 Hz, 2H, ArH), 8.17 (d, J_{HH} = 9.0 Hz, 1H, ArH), 8.56 (d, J_{HH} = 2.76 Hz, 1H, ArH), 8.57–8.60 (dd, J_{HH} = 2.28, 9.04 Hz, 1H, ArH), 8.84 (s, 1H, $CH_{pyrazole}$), 9.73 (s, 1H, OH); ^{13}C NMR (100 MHz, DMSO-d_6): δ_C 31.31, 115.59, 115.90, 116.23, 121.11, 122.43, 124.09, 127.18, 127.65, 129.27, 130.01, 132.18, 135.19, 135.61, 141.90, 144.60, 158.45, 169.40, 195.45; HRMS *m/z* (pos): 534.0612 $C_{21}H_{13}N_5O_7S_2Na$ (calcd: 534.0614).

(Z)-3-Acetyl-5-((1-(2,4-dinitrophenyl)-3-(3-methoxyphenyl)-1H-pyrazol-4-yl)methylene)-2-thioxothiazolidin-4-one (6e)

Yellow solid; Yield: 63%; mp 72.9–77.0 °C; FTIR ν_{max} (cm^{-1}): 3068.00 (C–H), 1684.57 (C=O), 1509.07 (NO_2), 1266.68 (C–O–C), 1185.97 (C=S), 1081.50 (C–N); ^{1}H NMR (400 MHz, DMSO-d_6): δ_H 3.80 (s, 1H, OCH_3), 4.25 (s, 3H, CH_3), 7.05 (s, 1H, $CH_{olefinic}$), 7.11 (d, J_{HH} = 7.92 Hz, 1H, ArH), 7.38 (s, 1H, ArH), 7.49 (d, J_{HH} = 7.84 Hz, 1H, ArH), 8.38 (d, J_{HH} = 8.88 Hz, 1H, ArH), 8.67 (t, J_{HH} = 7.40 Hz, 1H, ArH), 8.87 (s, 1H, $CH_{pyrazole}$), 8.89 (d, J_{HH} = 2.04 Hz, 1H, ArH); ^{13}C NMR (100 MHz, DMSO-d_6): δ_C 31.32, 55.19, 114.11, 114.89, 116.76, 120.41, 120.77, 121.12, 126.27, 126.74, 127.89, 130.28, 131.45, 131.92, 135.06, 142.76, 146.03, 154.77, 159.49, 168.88, 176.63, 194.70; HRMS *m/z* (pos): 548.9518 $C_{22}H_{15}N_5O_7S_2Na$ (calcd: 518.9508).

(Z)-3-Acetyl-5-((1-(2,4-dinitrophenyl)-3-(2-methoxyphenyl)-1H-pyrazol-4-yl)methylene)-2-thioxothiazolidin-4-one (6f)

Orange solid; Yield: 81%; mp 74.8–79.7 °C; FTIR ν_{max} (cm^{-1}): 3085.29 (C–H), 1705.29 (C=O), 1503.55 (NO_2), 1240.20 (C–O–C), 1175.78 (C=S), 1061.64 (C–N); ^{1}H NMR (400 MHz, DMSO-d_6): δ_H 3.88 (s, 3H, OCH_3),4.26 (s, 3H, CH_3), 7.10 (s, 1H, $CH_{olefinic}$), 7.20–7.28 (m, 3H, ArH), 7.55 (t, J_{HH} = 7.64 Hz, 1H, ArH), 8.40 (d, J_{HH} = 8.92 Hz, 1H, ArH), 8.65–8.68 (dd, J_{HH} = 1.8, 8.92 Hz, 1H, ArH), 8.84 (s, 1H, $CH_{pyrazole}$), 8.98 (d, J_{HH} = 1.8 Hz, 1H, ArH); ^{13}C NMR (100 MHz, DMSO-d_6): δ_C 31.32, 55.52, 112.10, 114.98, 118.12, 118.97, 120.92, 121.14, 124.84, 126.68, 127.92, 131.20, 131.31, 135.20, 140.58, 142.75, 145.94, 153.67, 156.65, 168.96, 176.64, 194.97; HRMS *m/z* (pos): 548.1798 $C_{22}H_{15}N_5O_7S_2Na$ (calcd: 548.1790).

(Z)-3-Acetyl-5-((3-(2,4-dichlorophenyl)-1-(2,4-dinitrophenyl)-1H-pyrazol-4-yl) methylene)-2-thioxothiazolidin-4-one (6g)

Orange solid; Yield: 79%; mp 71.6–75.2 °C; FTIR ν_{max} (cm^{-1}): 3084.67 (C–H), 1691.78 (C=O), 1532.18 (NO_2),

1177.34 (C=S), 1075.55 (C–N); ^{1}H NMR (400 MHz, DMSO-d_6): δ_H 4.26 (s, 3H, CH_3), 6.99 (s, 1H, $CH_{olefinic}$), 7.47 (d, J_{HH} = 8.24 Hz, 1H, ArH), 7.61–7.63 (dd, J_{HH} = 1.8, 8.24 Hz, 1H, ArH), 7.86 (d, J_{HH} = 1.76 Hz, 1H, ArH), 8.40 (d, J_{HH} = 8.92 Hz, 1H, ArH), 8.68–8.71 (dd, J_{HH} = 2.32, 8.92 Hz, 1H, ArH), 8.91 (d, J_{HH} = 2.44 Hz, 1H, ArH), 8.97 (s, 1H, $CH_{pyrazole}$); ^{13}C NMR (100 MHz, DMSO-d_6): δ_C 30.93, 117.90, 119.81, 121.16, 123.61, 126.15, 129.66, 131.91, 133.00, 133.49, 133.75, 135.08, 135.58, 137.49, 143.02, 146.34, 150.72, 152.31, 168.89, 176.63, 194.75; HRMS *m/z* (pos): 585.1322 $C_{21}H_{11}N_5O_6S_2Cl_2Na$ (calcd: 585.1327).

(Z)-3-Acetyl-5-((1-(2,4-dinitrophenyl)-3-(4-methoxyphenyl)-1H-pyrazol-4-yl)methylene)-2-thioxothiazolidin-4-one (6h)

Orange solid; Yield: 88%; mp 70.4–73.8 °C; FTIR ν_{max} (cm^{-1}): 3075.83 (C–H), 1708.98 (C=O),1536.98 (NO_2), 1250.24 (C–O–C), 1173.27 (C=S), 1075.91 (C–N); ^{1}H NMR (400 MHz, DMSO-d_6): δ_H 3.87 (s, 3H, OCH_3), 4.26 (s, 3H, CH_3), 7.12 (d, J_{HH} = 8.60 Hz, 2H, ArH), 7.34 (s, 1H, $CH_{olefinic}$), 7.47 (d, J_{HH} = 8.56 Hz, 2H, ArH), 8.37 (d, J_{HH} = 8.92 Hz, 1H, ArH), 8.64–8.67 (dd, J_{HH} = 2.12, 8.92 Hz, 1H, ArH), 8.85 (s, 1H, $CH_{pyrazole}$), 8.89 (d, J_{HH} = 2.44 Hz, 1H, ArH); ^{13}C NMR (100 MHz, DMSO-d_6): δ_C 31.31, 55.29, 114.57, 116.62, 121.12, 122.44, 126.05, 126.61, 127.87, 129.90, 131.00, 135.11, 142.70, 145.91, 154.90, 160.29, 160.29, 162.65, 168.92, 176.64, 194.92; HRMS *m/z* (pos): 548.1510 $C_{22}H_{15}N_5O_7S_2Na$ (calcd: 548.1502).

(Z)-3-Acetyl-5-((3-(3,4-dichlorophenyl)-1-(2,4-dinitrophenyl)-1H-pyrazol-4-yl) methylene)-2-thioxothiazolidin-4-one (6i)

Yellow solid; Yield: 61%; mp 80.2–84.0 °C; FTIR ν_{max} (cm^{-1}): 3076.56 (C–H), 1705.63 (C=O), 1531.05 (NO_2), 1180.64 (C=S), 1069.12 (C–N); ^{1}H NMR (400 MHz, DMSO-d_6): δ_H 4.26 (s, 3H, CH_3), 7.35 (s, 1H, $CH_{olefinic}$), 7.56 (d, J_{HH} = 8.64 Hz, 1H, ArH), 7.79 (d, J_{HH} = 15.72 Hz, 1H, ArH), 7.82 (s, 1H, ArH), 8.87 (d, J_{HH} = 8.32 Hz, 1H, ArH), 8.40 (d, J_{HH} = 8.88 Hz, 1H, ArH), 8.68–8.71 (dd, J_{HH} = 2.04, 8.72 Hz, 1H, ArH), 8.93 (d, J_{HH} = 2.2 Hz, 1H, ArH), 8.95 (s, 1H, $CH_{pyrazole}$); ^{13}C NMR (100 MHz, DMSO-d_6): 28.95, 111.38, 113.88, 114.81, 119.54, 119.61, 120.71, 122.37, 123.21, 124.08, 125.71, 126.16, 131.44, 133.89, 136.93, 143.73, 148.40, 166.21, 176.67, 189.28; HRMS *m/z* (pos): 585.0106 $C_{21}H_{11}N_5O_6S_2Cl_2Na$ (calcd: 585.0093).

General procedure for the synthesis of (Z)-3-acetyl-5-benzylidene-2-thioxothiazolidin-4-ones (8a–e)

Appropriate aromatic aldehydes (**7a–e**) (0.01 mmol), rhodanine (**5**) (0.012 mmol) and anhydrous sodium acetate (0.03 mmol) were dissolved in 15 mL of acetic acid and refluxed for 3 h. Once TLC confirmed the completion of the reaction, solvent was removed using a high vacuum. The reaction mixture was then poured on crushed ice and the obtained solid was filtered and purified using column chromatography.

(Z)-3-Acetyl-5-benzylidene-2-thioxothiazolidin-4-one (8a)

Yellow solid; Yield: 93%; mp 141.2–145.4 °C; FTIR ν_{max} (cm^{-1}): 3076.31 (C–H), 1704.57 (C=O), 1185.29 (C=S), 1082.27 (C–N); ^{1}H NMR (400 MHz, DMSO-d_6): δ_H 4.26 (s, 3H, CH_3), 7.50–7.61 (m, 5H, ArH), 7.64 (s, 1H, $CH_{olefinic}$); ^{13}C NMR (100 MHz, DMSO-d_6): δ_C 30.75, 125.54, 129.42, 130.44, 130.71, 131.58, 132.94, 169.41, 176.66, 195.72; HRMS *m/z* (pos): 288.0928 $C_{12}H_9NO_2S_2Na$ (calcd: 288.0929).

(Z)-3-Acetyl-5-(4-methoxybenzylidene)-2-thioxothiazolidin-4-one (8b)

Yellow solid; Yield: 80%; mp 195–196 °C; FTIR ν_{max} (cm^{-1}): 3054.83 (C–H), 1682.73 (C=O), 1257.71 (C–O–C), 1169.05 (C=S), 1073.09 (C–N); ^{1}H NMR (400 MHz, DMSO-d_6): δ_H 3.83 (s, 3H, OCH_3), 4.26 (s, 3H, CH_3), 7.12 (d, J_{HH} = 8.70 Hz, 2H, ArH), 7.58 (d, J_{HH} = 8.70 Hz, 2H, ArH), 7.61 (s, 1H, $CH_{olefinic}$); ^{13}C NMR (100 MHz, DMSO-d_6): δ_C 31.63, 55.54, 115.08, 122.18, 125.45, 131.88, 132.67, 161.33, 169.38, 176.65, 195.47; HRMS *m/z* (pos): 318.0330 $C_{13}H_{11}NO_3S_2Na$ (calcd: 318.0331).

(Z)-3-Acetyl-5-(2-chlorobenzylidene)-2-thioxothiazolidin-4-one (8c)

Yellow solid; Yield: 87%; mp 170.0–174.5 °C; FTIR ν_{max} (cm^{-1}): 3054.53 (C–H), 1693.30 (C=O), 1184.14 (C=S), 1040.24 (C–N); ^{1}H NMR (400 MHz, DMSO-d_6): δ_H 4.26 (s, 3H, CH_3), 7.49–7.54 (m, 3H, ArH), 7.64 (t, J_{HH} = 5.20 Hz, 1H, ArH), 7.74 (s, 1H, $CH_{olefinic}$); ^{13}C NMR (100 MHz, DMSO-d_6): δ_C 30.93, 126.07, 128.24, 129.05, 129.27, 130.41, 130.81, 132.07, 134.73, 169.10, 176.64, 195.51; HRMS *m/z* (pos): 321.0585 $C_{12}H_8NO_2S_2ClNa$ (calcd: 321.0591)

(Z)-3-Acetyl-5-(3-chlorobenzylidene)-2-thioxothiazolidin-4-one (8d)

Yellow solid; Yield: 92%; mp 165–167 °C; FTIR ν_{max} (cm^{-1}): 3078.09 (C–H), 1704.77 (C=O), 1181.24 (C=S), 1079.59 (C–N); ^{1}H NMR (400 MHz, DMSO-d_6): δ_H 4.26 (s, 3H, CH_3), 7.53–7.57 (m, 3H, ArH), 7.63 (s, 1H, ArH) 7.68 (s, 1H, $CH_{olefinic}$); ^{13}C NMR (100 MHz, DMSO-d_6): δ_C 29.70, 127.36, 128.10, 129.76, 130.21, 130.26, 131.22,

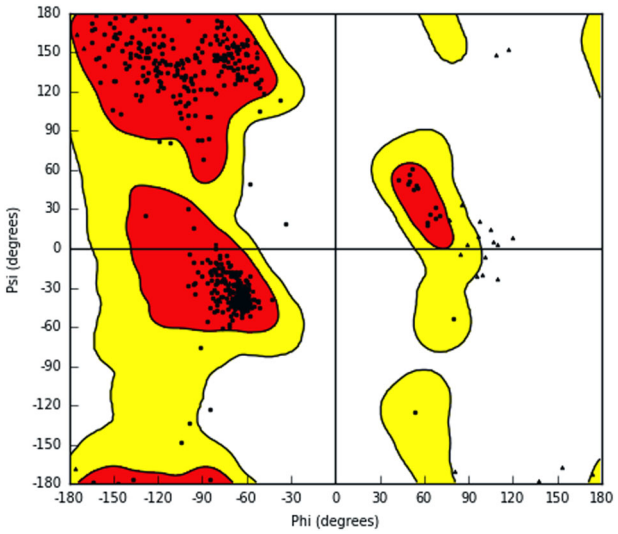

Fig. 3 Ramachandran plot

134.01, 135.12, 169.27, 176.66, 195.38; HRMS *m/z* (pos): 319.0590 $C_{12}H_8NO_2S_2ClNa$ (calcd: 319.0591).

(Z)-3-Acetyl-5-(2,5-dimethoxybenzylidene)-2-thioxothiazolidin-4-one (8e)

Yellow solid; Yield: 96%; mp 140–142 °C; FTIR ν_{max} (cm^{-1}): 3067.11 (C–H), 1704.37 (C=O), 1184.97 (C=S), 1184.97 (C–O), 1080.99 (C–N); ^{1}H NMR (400 MHz, DMSO-d_6): δ_H 3.83 (s, 6H, OCH_3), 4.26 (s, 3H, CH_3), 7.12–7.21 (m, 3H, ArH), 7.61 (s, 1H, $CH_{olefinic}$); ^{13}C NMR (100 MHz, DMSO-d_6): δ_C 30.92, 55.52, 56.03, 113.12, 113.81, 118.47, 121.72, 125.62, 126.62, 152.52, 153.15, 169.32, 184.62, 195.81; HRMS *m/z* (pos): 346.1361 $C_{14}H_{13}NO_4S_2Na$ (calcd: 346.1372).

Antidiabetic activity testing methods

Determination of α-glucosidase inhibitory activity

The α-glucosidase inhibitory activities for the synthesised compounds were determined using a modified method described by Ademiluyi and Oboh (2013). Briefly, 100 µL of 1.0 U/mL of α-glucosidase, in a phosphate buffer (100 mM, pH 6.8), with 50 µL of each synthesised compounds, or acarbose, dissolved in ethanol to obtain different concentrations (15, 30, 60, 120 and 240 µg/mL), was incubated in a 96-well plate at 37 °C for 20 min. Thereafter 50 µL of 5 mM of *p*-nitrophenyl-α-D-glucopyrnoside (pNPG) solution was added to the reaction mixture and was further incubated at 37 °C for 30 min. The absorbance was then measured at 405 nm and the results expressed as a percentage of the control sample without inhibitors by the formula:

$$\%\text{inhibition} = \left[\left(\begin{array}{c}\text{absorbance of blank} - \\ \text{absorbance of compound}\end{array}\right)/\text{absorbance of blank}\right] * 100$$

Determination of α-amylase inhibitory activity

The α-amylase inhibitory activity of the synthesised compounds were determined using a modified method described by Shai et al. (2010), in which 250 µL of each synthesised compound, or acarbose, dissolved in ethanol to obtain different concentrations (15, 30, 60, 120 and 240 µg/mL), was mixed with 500 µL of porcine pancreatic amylase (2 U/mL) in phosphate buffer (100 mM, pH 6.8) and incubated for 10 min at 37 °C. Thereafter, 50 µL of 1% starch, dissolved in the same buffer, was added to the reaction mixture and the samples were incubated again at 37 °C. After 30 min, dinitrosalicylate (DNS) colour reagent (1 mL) was and the samples were allowed to boil for 10 min. Absorbance was then measured at 540 nm. The results were expressed as a percentage of the control by the formula below:

$$\%\text{inhibition} = \left[\left(\begin{array}{c}\text{absorbance of blank} - \\ \text{absorbance of compound}\end{array}\right)/\text{absorbance of blank}\right] * 100$$

Homology modelling

The protein sequence of *Saccharomyces cerevisiae* α-glucosidase was obtained from UniProt (http://www.uniprot.org) with accession number P53341. X-ray crystal structure of *S. cerevisiae* isomaltase (PDB ID code 3AJ7 of 1.30 Å resolution) having a 72.4% sequence identity with *S. cerevisiae* α-glucosidase was selected as a template for the homology modelling as employed in previous studies (Guerreiro et al. 2013; Khan et al. 2014). The query and template sequence were aligned using the pairwise sequence alignment tool of ClustalOmega. The three-dimensional (3D) structural model of α-glucosidase for *S. cerevisiae* was obtained by homology modelling using MODELER 9.19 integrated in Chimera (Sievers and Higgins 2014; Webb and Sali 2014; Pettersen et al. 2004). The model with the lowest discrete optimized protein energy (DOPE) score was selected for validation.

The modelled *S. cerevisiae* α-glucosidase structure was validated by generating the phi/psi Ramachandran plot (Fig. 3) distributions obtained by using protein preparation wizard of Schrodinger modelling suite and RAMPAGE Ramachandran plot analysis server. In addition, the significance consistency between the modelled structure and the selected template was evaluated using ProSA server

Scheme 1 Synthetic pathway of pyrazole–rhodanine hybrids (**6a–i**)

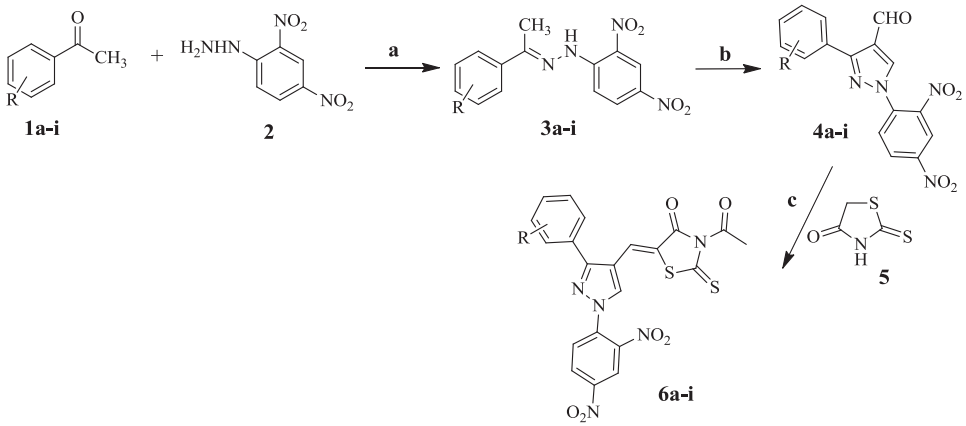

Reagents and conditions: (a) EtOH, H_2SO_4, RT, 1 h; (b) DMF, $POCl_3$, 60 °C, 5 h; (c) AcONa, AcOH, EtOH, reflux, 3 h.

(Sastry et al. 2013; Lovell et al. 2003; Wiederstein and Sippl 2007).

Molecular docking method

Prior to molecular docking, a total of 5000 steps of energy minimization were performed for the modelled structure using Amber14 force field of AMBER 14 molecular dynamic simulation package (Case et al. 2014; Trott and Olson 2010). Molecular docking was performed using Autodock Vina software package integrated in Chimera software. The software's default settings were used for the docking procedures. A Chimera graphical user interface tool was used to assign Geister partial charges during the docking process. The binding site pocket of *S. cerevisiae* α-glucosidase for molecular docking was defined by a grid box around key active site residues Glu276, Asp214, Asp349, Arg439, Arg312, Asp408, Gln350, Ser438, Val108, Phe157, Phe177 and Phe300 of the minimized α-glucosidase modelled structure. The *X*, *Y* and *Z* dimensions were defined as 26.0448, 24.4198, and 27.4387, respectively whereas the *X*, *Y* and *Z* centres were defined by 34.4671, 46.5256 and 49.559, respectively. Polar hydrogens were assigned for all compounds. The docked complex structures were visualized by the UCSF chimera graphical user interface and molecular interactions were also visualized using Molegro Molecular Viewer (http://www.clcbio.com).

Results and discussion

Chemistry

Synthesis of the molecular hybrids (**6a–i**) and simple rhodanine analogues (**8a–e**) has been outlined in Schemes 1 and 2. The MH reported herein consists of two steps, the synthesis of the pyrazole aldehyde derivatives which is a key intermediate for further transformation, followed by coupling of these derivatives with commercially available rhodanine. The pyrazole aldehydes (**4a–i**) were achieved by cyclisation of the synthesized hydrazone intermediates (**3a–i**). Specifically, the reaction of appropriate substituted acetophenones (**1a–i**) with 2,4-dinitrophenylhydrazine (**2**) was conducted in the presence of sulfuric acid in absolute ethanol and water to afford the hydrazone intermediates (**3a–i**). The synthesized hydrazone intermediates then undergo a Vilsmeier–Hack reaction (DMF-$POCl_3$) at 80 °C for 5 h to afford pyrazole aldehydes (**4a–i**) (Andleeb et al. 2016). The pyrazole–rhodanine hybrid compounds (**6a–i**) were prepared via a Knoevenagel condensation of rhodanine (**5**) with the synthesised pyrazole aldehydes (**4a–i**), by refluxing both in acetic acid, in the presence of a catalytic amount of sodium acetate for 3 h. The same mechanistic pathway and reaction conditions were used to synthesize (Z)-3-acetyl-5-benzylidene-2-thioxothiazolidin-4-ones (**8a–e**) via the reaction of various substituted aromatic aldehydes (**7a–e**) with rhodanine.

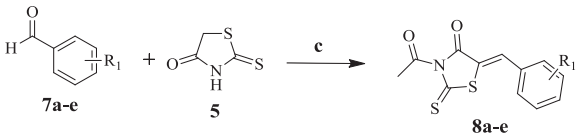

Scheme 2 Synthesis of substituted phenyl–rhodanine hybrids (**8a–e**)

After purification, the structure of all the synthesized compounds were characterized using spectroscopic techniques (IR, HRMS, ^{1}H and ^{13}C NMR). For example, the ^{1}H NMR of compound **6b** exhibits three singlets. The most characteristic singlet appeared at δ 7.37 ppm which corresponds to the one vinylic proton (=CH) between the

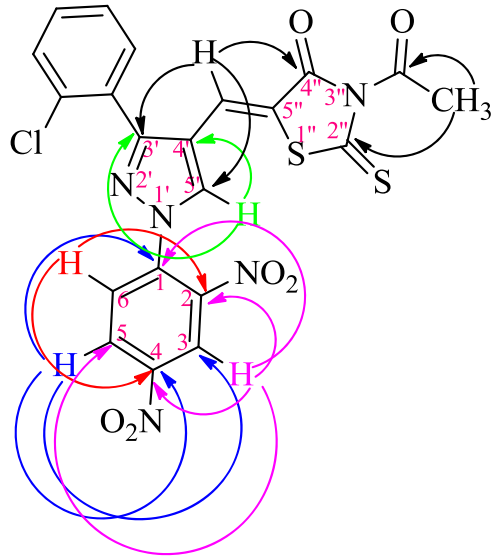

Fig. 4 HBMC ($^{1}H \rightarrow ^{13}C$) correlation of compound **6b**

pyrazole and rhodanine moieties. The other two singlets are seen at δ 8.92 ppm and δ 4.26 ppm which correspond to the proton in the pyrazole ring, and three protons of N-acetyl group attached to the rhodanine respectively. *J* coupling was then used to assign the protons present in the 2,4-dinitrophenyl ring, which were seen to be highly deshielded, and therefore downfield, due to the presence of the two nitro groups. The doublet at δ 8.40 ppm corresponds to H-6 and is *ortho* coupled to H-5 ($J_{HH} = 8.88$ Hz). On the other hand, H-5 is a doublet of doublets at δ 8.67 ppm and is *ortho* coupled to H-6 and *meta* coupled to H-3 ($J_{HH} = 2.44$, 8.88 Hz). H-3 appeared as a doublet at δ 8.91 ppm ($J_{HH} =$ 2.44 Hz) and is the most downfield proton due to it being in-between two nitro groups. A multiplet is also seen in the region of δ 7.54–7.57 ppm, which corresponds to the four protons in the chloro substituted phenyl ring. Along with coupling constants, COSY was also used to confirm the assignment of the proton peaks, especially those of the 2,4-dinitrophenyl ring.

Although, hypothetically, two geometric isomers, E and Z, are probable for the Knoevenagel condensed products, all the compounds displayed only the Z-configuration, as anticipated from reported studies, which is confirmed by the peak for =CH appeared between 6.98 and 7.74 ppm in the ^{1}H NMR spectra, as the vinylic proton is more deshielded in the Z-isomer than the E-isomer due to the magnetic anisotropy effects of the carbonyl group on the vinylic proton. Hence, Z-configuration due to the high degree of thermodynamic stability attributed to intramolecular hydrogen bond that can be formed between the rhodanine carbonyl oxygen atom and the =CH group of hydrogen atom (Mendoza et al. 2014; Kumar and Nanjan 2010; Mandal et al. 2016).

Additionally, these assignments were supported by heteronuclear multiple bond correlation (HMBC) correlations, selected HMBC correlations used in the structural elucidation of **6b** are provided in Fig. 4. The structure of **6b** was further confirmed by the ^{13}C NMR in which the most characteristic peak at δ 31.32 ppm corresponding to the methyl carbon, and the peak at δ 121.15 ppm which corresponds to vinylic carbon. The most deshielded peaks at δ 194.93 and 168.91 ppm correspond to the thiocarbonyl (which is correlation with acetyl group protons) and carbonyl (which is correlation with vinylic proton) in the rhodanine ring, respectively. Whereas, the acetyl carbonyl functional group resonated in the region 176.64 ppm, these peaks, along with the other 16 peaks seen in the ^{13}C NMR were confirmed using HMBC and HSQC spectra.

These results suggested Knoevenagel condensation obtained between pyrazole aldehyde and rhodanine, as well as the presence of the acetyl carbon peak and the methyl carbon peak in the ^{13}C NMR and acetyl protons peak in ^{1}H NMR spectra confirms that acetylation occurred in the synthesis of the pyrazole–rhodanine derivatives. Furthermore, the IR spectrum of compound **6b** showed characteristic absorption peak exhibited at 1700.31 and 1172.16 cm^{-1} due to the (C=O) and (C=S) groups, respectively. The successful synthesis of **6b** was further supported by HRMS in which the molecular-ion peak was found at $m/z = 551.9636$.

In vitro α-glucosidase and α-amylase inhibitory activity

Two different molecular hybrid scaffolds were synthesized, namely the pyrazole–rhodanine scaffolds (**6a–i**) and the phenyl–rhodanine scaffolds (**8a–e**). This was done to allow the comparison of the two different scaffolds, in terms of their antidiabetic activity, with the hope that the pyrazole–rhodanine scaffold would have a significantly better activity as it possesses two pharmacophores. The antidiabetic activities of the synthesized compounds were determined via in vitro testing against the α-glucosidase and α-amylase enzymes, from which the IC_{50} values were determined and compared to the standard reference drug, acarbose. The IC_{50} values of each compound obtained from both inhibitory studies summarized in Table 1.

For the inhibition of the α-glucosidase enzyme, the IC_{50} values of the synthesized compounds (**6a–i** and **8a–e**) were compared to that of acarbose ($IC_{50} = 9.667 \times 10^{-5}$ mol/L). Compounds **6a–i** exhibited better α-glucosidase inhibitory activity compared to acarbose, with IC_{50} values ranging from 2.259×10^{-6} to 1.160×10^{-4} mol/L. Although, the IC_{50} values of compounds **8a–e** ranged between 3.086×10^{-4} and $> 9.494 \times 10^{-4}$ mol/L. For the α-amylase inhibitory activity, the synthesized compounds exhibited good inhibition with a

Table 1 In vitro IC_{50} values of α-glucosidase and α-amylase inhibition activities of synthesised compounds **6a–i** and **8a–e**

compounds **6a-i** and **8a-e**.

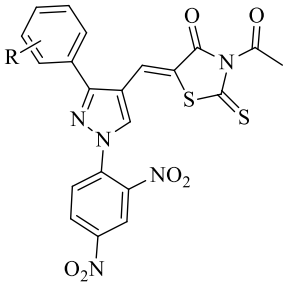

Compounds 6a-i

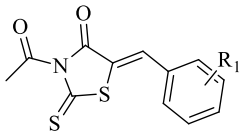

Compounds 8a-e

Comp.	Structures	IC_{50} (mol/L)	
		α-Glucosidase	α-Amylase
6a	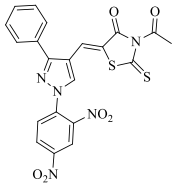	2.854×10^{-5}	3.227×10^{-4}
6b	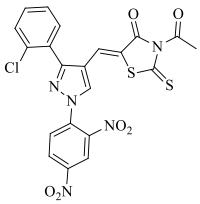	3.491×10^{-5}	7.729×10^{-4}
6c	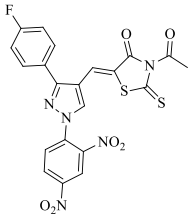	1.065×10^{-4}	3.093×10^{-4}
6d	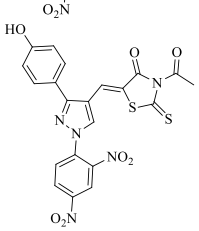	2.099×10^{-5}	6.377×10^{-5}
6e	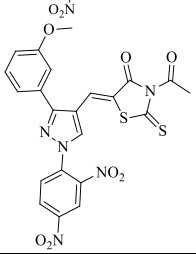	4.116×10^{-5}	3.680×10^{-4}

6f	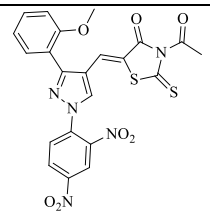	2.259×10^{-6}	3.080×10^{-4}
6g	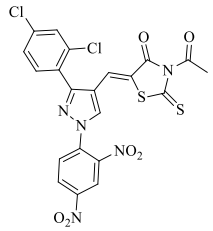	6.183×10^{-5}	1.693×10^{-4}
6h	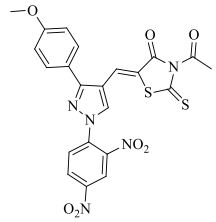	1.160×10^{-4}	1.325×10^{-4}
6i	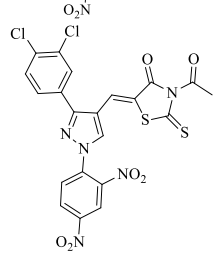	6.383×10^{-5}	2.231×10^{-4}
8a	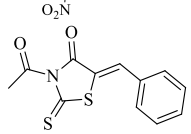	$>9.494 \times 10^{-4}$	6.251×10^{-4}
8b	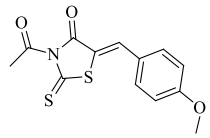	3.086×10^{-4}	3.439×10^{-4}
8c	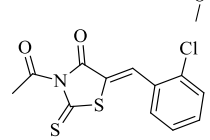	3.809×10^{-4}	$>8.395 \times 10^{-4}$
8d	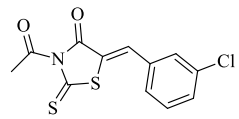	$>8.395 \times 10^{-4}$	$>8.395 \times 10^{-4}$
8e	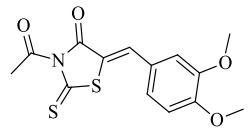	7.623×10^{-4}	3.114×10^{-4}
Standard	**Acarbose**	9.667×10^{-5}	1.038×10^{-4}

range of IC_{50} values from 6.377×10^{-5} to 7.730×10^{-4} mol/L and 3.114×10^{-4} to 6.251×10^{-4} mol/L, for **6a–i** and **8a–e**, respectively, with acarbose having an IC_{50} value of 1.038×10^{-4} mol/L. Unlike the α-glucosidase inhibitory activity, only a slight difference is observed between the α-amylase inhibitory activity of the pyrazole–rhodanine derivatives (**6a–i**) and the substituted phenyl–rhodanine derivatives (**8a–e**). However, there were certain pyrazole–rhodanine derivatives that showed good inhibitory activity. This proves that the presence of the pyrazole ring, and possibly the nitro groups present on the phenyl ring adds to the inhibitory activity of the pyrazole–rhodanine series.

Although all the structural features, for instance, the pyrazole ring and N-acetyl rhodanine moieties, are pleasantly playing their part in signifying the inhibitory potential, the variation of the substituents in the phenyl ring on the pyrazole moiety was seen to result in a large range of IC_{50} values. A structural assessment was conducted to examine the effects of the different substitution at the aryl moiety (R) of the pyrazole–rhodanine derivatives.

In terms of the α-glucosidase inhibitory activity, compounds **6f** ($IC_{50} = 2.259 \times 10^{-6}$ mol/L), **6e** ($IC_{50} = 4.116 \times 10^{-5}$ mol/L) and **6h** ($IC_{50} = 1.160 \times 10^{-4}$ mol/L), which all contain a methoxy group at phenyl ring, showed potent activity, with **6f** having a 42-fold stronger potency than the standard acarbose ($IC_{50} = 9.667 \times 10^{-5}$ mol/L). The enhanced activity of compound **6f** may be due to the presence of an electron donating methoxy group at the *ortho* position, which may be responsible for its binding with the α-glucosidase enzyme. In comparison, the relatively decreased activity of compounds **6e** and **6h** may be due to the change in the position of methoxy group from *ortho* to *meta* and *ortho* to *para*, respectively, which were approximately 18-fold and 51-fold less potent than that of compound **6f**, respectively. The replacement of the methoxy group with an electron withdrawing chloro group at *ortho* position (**6b**) reduced the inhibitory efficacy, but still showed an inhibitory activity 2-fold higher than the standard inhibitor. The *ortho* position was again favoured for the chloro substituents, with the 2-chloro substituted phenyl of pyrazole derivative (**6b**) displaying good inhibitory activity, with an IC_{50} value of 3.491×10^{-5} mol/L, while the 2,4-dichloro (**6g**) and 3,4-dichloro (**6i**) substituted derivatives displayed IC_{50} values of 6.183×10^{-5} mol/L and 6.383×10^{-5} mol/L, respectively. This also shows that the mono chloro-substituted derivative was favoured over a dichloro substituted derivative. It is also interesting to note that the unsubstituted derivative (**6a**) showed the second highest activity, with an IC_{50} value of 2.854×10^{-4} mol/L, which is more than 3-fold better than that of acarbose. Compounds containing *para* hydroxy (**6d**; $IC_{50} = 2.099 \times 10^{-5}$ mol/L) and *para* fluoro (**6c**; $IC_{50} = 1.065 \times 10^{-4}$ mol/L) substituted phenyl rings on the pyrazole moiety were also found to be active. On the other hand, when the pyrazole moiety was changed to the substituted phenyl moiety, the resulting compounds, **8a–e**, displayed less inhibitory activity against the α-glucosidase enzyme. However, in the case of compound **8b** ($IC_{50} = 3.086 \times 10^{-4}$ mol/L), where the 4-methoxy group was present, the derivative showed the highest inhibition of the α-glucosidase enzyme. The difference in activity displayed between the two series of derivatives suggests that the pyrazole moiety might be helpful in the binding of the pyrazole–rhodanine derivatives with the active site of the α-glucosidase enzyme.

In the case of the α-amylase inhibition activity, compound **6d**, which is the *para*-hydroxy substituted pyrazole–rhodanine derivative, exhibited the highest inhibitory activity, with an IC_{50} value of 6.377×10^{-5} mol/L, which is approximately 1.5-fold higher than acarbose ($IC_{50} = 1.038 \times 10^{-4}$ mol/L). The 4-methoxy substituted derivative (**6h**) had the second highest inhibitory activity, with an IC_{50} value of 1.325×10^{-4} mol/L. When comparing the position of the electron donating methoxy group attached to the phenyl ring on the pyrazole moiety, the 4-methoxy substituted derivative (**6h**) was found to be more active than the 2-methoxy (**6f**) and 3-methoxy (**6e**) derivatives which had IC_{50} values of 3.080×10^{-4} and 3.680×10^{-4} mol/L, respectively. In contrast, when looking at the electron withdrawing chloro group on the phenyl ring on the pyrazole moiety, the 2,4-dichloro substituted derivative **6g** had a higher activity ($IC_{50} = 1.693 \times 10^{-4}$ mol/L) than the 3,4-dichloro (**6i**) and 2-chloro (**6b**) derivatives (IC_{50} value of 2.231×10 and 7.730 mol/L, respectively). Compounds **6a**, which is an unsubstituted derivative, and **6c**, the 4-fluoro substituted derivative, were found to be moderately active (IC_{50} values of 3.227×10^{-4} and 3.093 mol/L respectively). Furthermore, all the substituted phenyl–rhodanine derivatives (**8a–e**) displayed moderate to weak activity with IC_{50} values ranging from 3.114×10^{-4} to 6.251×10^{-4} mol/L. Thus, it can be seen from the results that the presence of the pyrazole moiety in the pyrazole–rhodanine derivatives is essential for the potent inhibitory activity compared to the substituted phenyl–rhodanine derivatives for both α-glucosidase and α-amylase inhibition. In general, the present study explored a new class of α-glucosidase inhibitors based on pyrazole–rhodanine compounds. Figure 5 provides a concise summary of the structural analysis potentially related to the activity.

Molecular docking

The homology model of glucosidase was validated using reported methods. Docking calculations of most active inhibitors were carried out against the homology built enzyme. For comparison, molecular docking of standard inhibitor acarbose was also carried out.

Analysis of the binding profile of acarbose in the active site of α-glucosidase (PDB ID: 5NN8) highlights significant

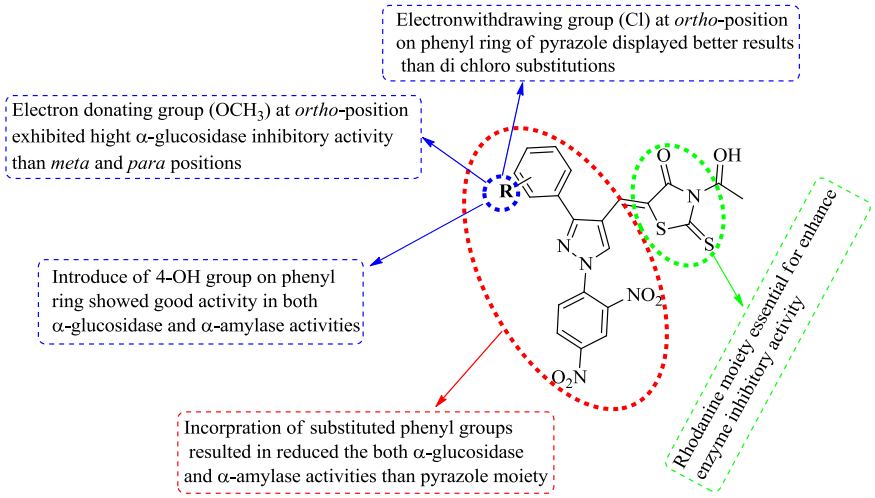

Fig. 5 Structural analysis of substituted phenyl of pyrazole–rhodanine derivatives as potent antidiabetic agents

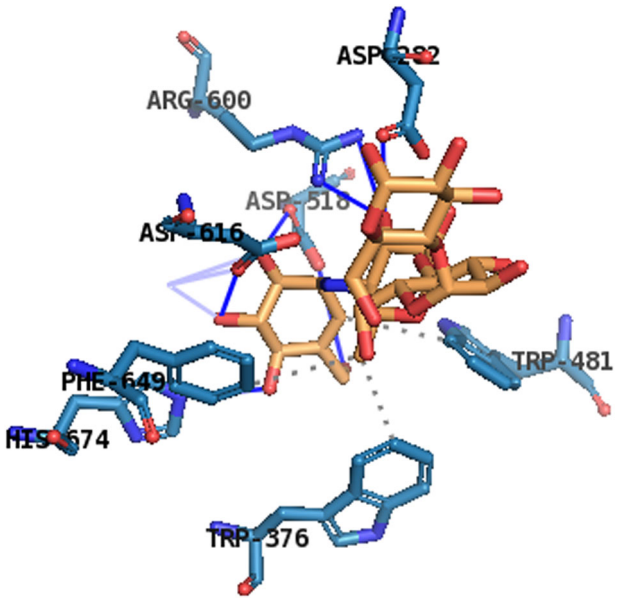

Fig. 6 Acarbose interacting with active site residues of α-glucosidase (PDB ID: 5NN8)

contribution by hydrogen bonds with two substrate subunits (subunit 1—represented as X_a, and subunit 2—X_b, where X is the residue identifier) (Fig. 6). These interactions are observed between residues $Asp91_a$, $Gly123_a$, $Trp126_a$, $Cys127_a$, $Asp282_b$, $Asp518_b$, $Arg600_b$, $Asp616_b$ and $His674_b$. The bond distance between the proton and acceptor measured 2.55, 2.42, 2.87, 1.81/2.29, 2.27, 3.14/3.24, 1.89/2.97 and 3.14 Å, respectively; with a bond angle of 113.5°, 161.3°, 105.6°, 142.9/110.0°, 145.7°, 136.3/115.2°, 179.1/129.7°, 125.0° and 171.9°, respectively. Acarbose is a pseudo tetrasaccharide comprising of four six-membered rings linked in a single chain which facilitates a hydrophobic interaction within the binding pocket between residues $Trp126_a$, $Trp376_b$, $Trp481_b$ and $Phe649_b$ (interaction distance of 3.60/3.99, 3.90, 3.99 and 3.97 Å, respectively). The second subunit of acarbose positioned in the binding pocket of α-glucosidase forms a water bridge between the surrounding solvent and donor residue Asp616 at an angle of 117.3° and 83.5° and donor–water distance of 2.85 Å.

The binding of acarbose to α-amylase (PDB ID: 2QV4) is more comprehensive and stabilized by predominantly hydrogen bond interactions (Fig. 7). The residues involved include hydrogen bond donors: Gln63 and Arg195 (bond distance = 1.69 and 2.11 Å; bond angle = 126.2° and 142.3°, respectively); as well as the hydrogen bond acceptors: Gln63, Ala106, Gly164, Glu233, Asp300 and His305 (bond distance = 2.90, 1.87, 2.53, 2.68/2.47, 2.23/2.40 and 3.09 Å, respectively; bond angle = 103.0°, 153.3°, 139.9°, 137.7/138.4°, 140.9/145.8° and 151.5°, respectively). Similar to the binding of acarbose to α-glucosidase, the α-amylase complex forms three water bridges with the surrounding solvent and amino acid residues Asn105, Ile235 and Asn298 (distance between donor and water = 3.22, 3.66 and 2.90 Å, respectively; water angle = 101.4°, 83.56° and 75.89°, respectively).

From elucidation of the binding profile of acarbose to the two enzyme binding pockets, it is evident that to ensure selective inhibition and maintain reversibility of ligand–protein complexation there needs to be a significant contribution from hydrogen bond interactions. The molecular docking of synthesized ligands was performed on a homology model of α-glucosidase built from *S. cerevisiae* α-glucosidase (Fig. 8). The model was validated according to the experimental method outlined in homolgy modelling section.

Compounds **8a–e** displayed no measurable activity against α-glucosidase. The measured total polar surface area (TPSA) of compounds **8a–e** is significantly lower than that for **6a–i** which relates to the poor solubility of the **8a–e**

derivatives (Table 2). This reduces their bioavailability and subsequent activity against α-glucosidase. As mentioned earlier, an extensive hydrogen bond interaction network facilitates potent inhibition of the enzyme, due to the lack of polarity of the ligands there is poor interaction between the ligand and protein.

Compounds **6a** and **6f** displayed the most potent inhibitory activity against α-glucosidase. The binding interaction profile of **6a** (Fig. 9) comprises a significant hydrogen bond contribution from the donor side chain of residues: Arg212 (amine group), Thr215 (hydroxyl group), Asn241 (amine group), Asp349 (carboxyl group) and Arg439 (amine group) (bond distance = 3.70/2.59, 2.28, 2.20, 3.35 and 3.58 Å, respectively; bond angle = 104.6/104.2°, 130.8°, 132.2°, 115.2° and 109.8°, respectively) with the oxygen of the nitro groups of the ligand. Three distinct hydrophobic interactions were observed between the conjugated rings and residues Phe157 and Arg312 at a distance of 3.64, 3.60 and 3.74 Å, respectively. A T-shaped π-stacking interaction is measured between Phe177 at 5.05 Å and angle of 74.43°. Compound **6f** (Fig. 9) displays a similar interaction profile; however, the binding of the ligand is supported by a greater contribution from hydrophobic interactions. These include residue binding with Phe157, Phe300, Pro309 and Arg312 (bond distance = 3.30/3.19/3.65/3.87, 4.00, 3.94 and 3.84 Å). Three hydrogen bonds exist between residues Arg212 (amine group), Asn241 (amine group) and Asp349 (carboxyl group) and

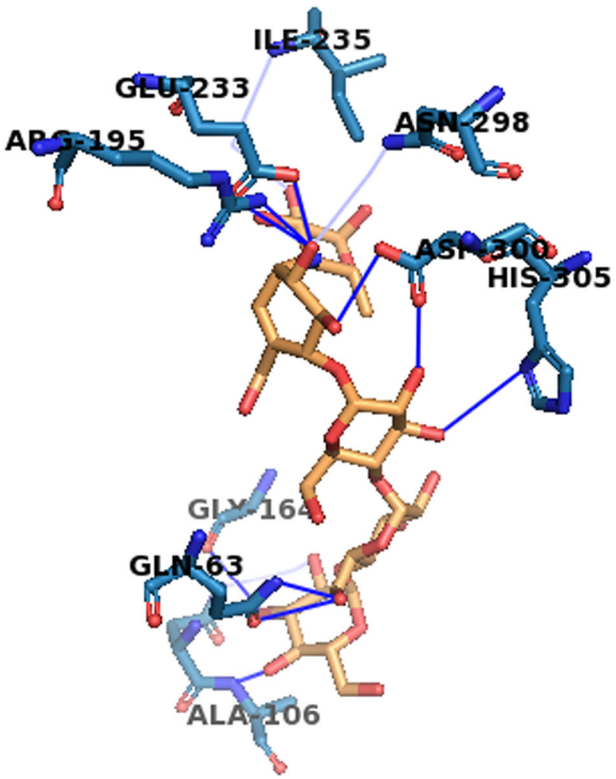

Fig. 7 Active site residues of α-amylase (PDB ID: 2QV4) interacting with acarbose

Table 2 Docking scores of synthesised compounds **6a–i** and **8a–e** in the homology model of α-glucosidase as well as their clogP and total polar surface area

Entry	Compound ID	Docking scores (kcal/mol)	clogP	TPSA (Å^2)
1	**6a**	−10.8	4.176	158.300
2	**6b**	−11.1	4.829	158.300
3	**6c**	−11.2	4.315	158.300
4	**6d**	−10.9	3.294	180.220
5	**6e**	−11.1	4.185	167.530
6	**6f**	−11.0	5.483	158.300
7	**6g**	−10.9	5.483	158.300
8	**6h**	−10.7	4.185	167.530
9	**6i**	−10.9	5.483	158.300
10	**8a**	−8.00	2.443	46.610
11	**8b**	−8.00	2.434	37.380
12	**8c**	−8.30	3.088	37.380
13	**8d**	−8.60	3.088	37.380
14	**8e**	−8.20	2.451	55.840

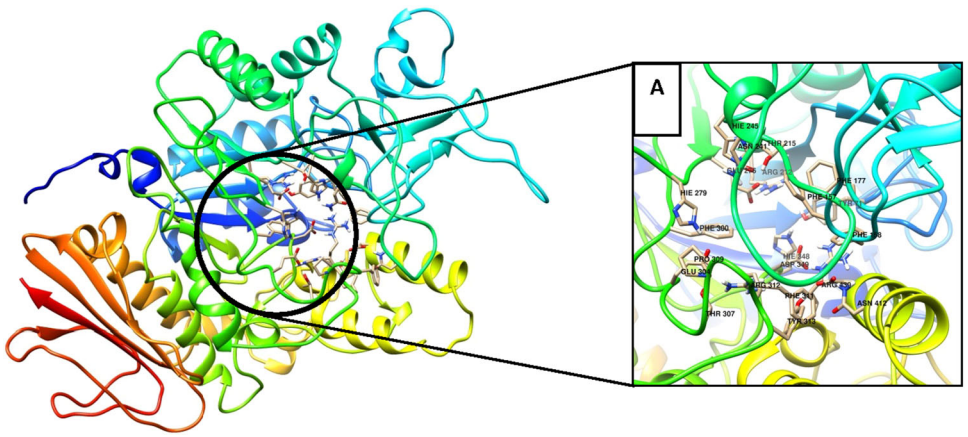

Fig. 8 3D representation of the homology model of α-glucosidase highlighting the catalytic site (**A**)

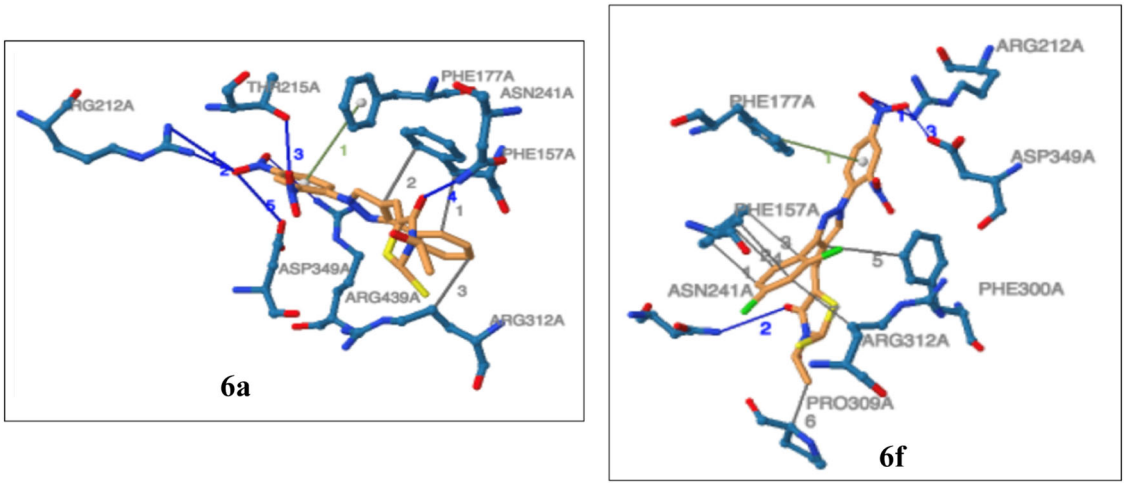

Fig. 9 Structure of **6a** and **6f** highlighting critical interactions in the enzyme active site

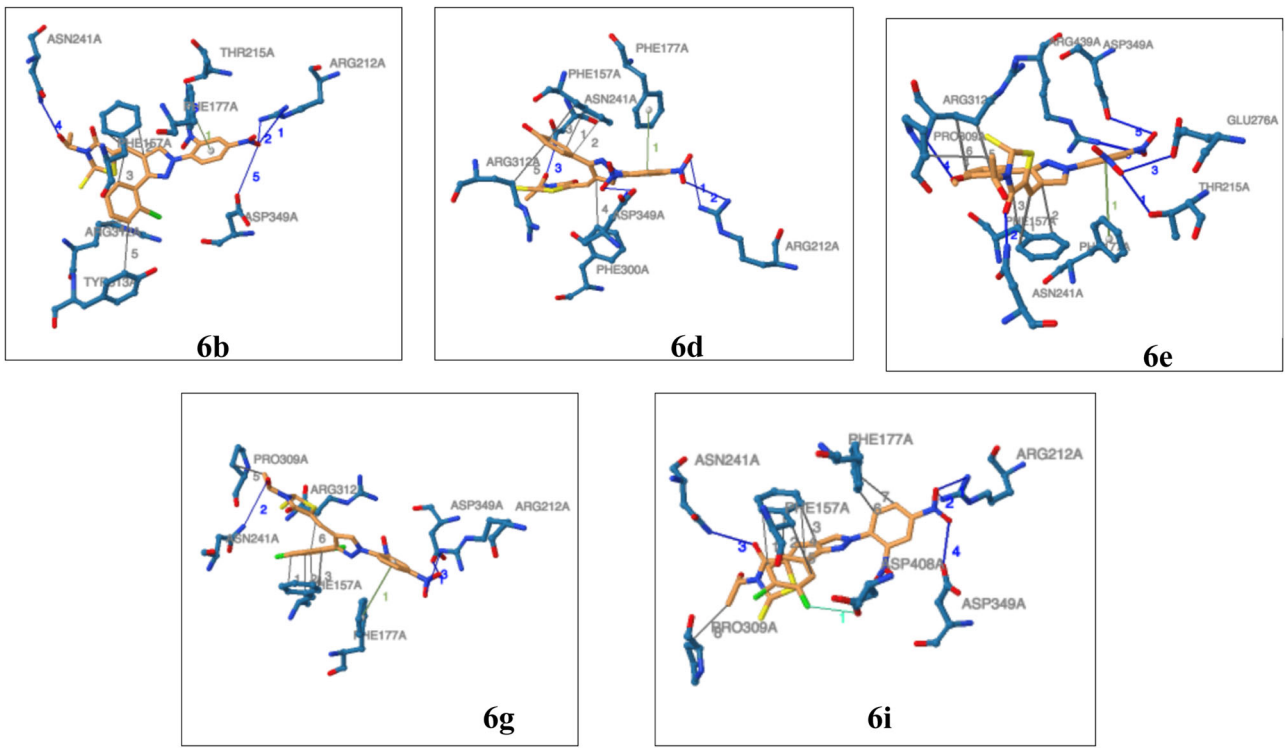

Fig. 10 Structure of **6b**, **6d**, **6e**, **6g** and **6i** interacting with α-glucosidase binding pocket residues

oxygen of the nitro groups of the ligand (bond distance = 3.19, 3.26 and 3.20 Å, respectively; bond angle = 152.8°, 105.2° and 115.3°, respectively). A T-shaped π-stacking is exerted by the conjugate rings and residue Phe177 at 4.82 Å and angle of 69.6°. The presence of the strongly activating electron-donating group at position 2 of the conjugated ring in **6f** improves the potency of the antidiabetic drug candidate, thus substitution at this position with primary and secondary amines and other alkoxide groups may improve efficacy, i.e. inhibitory activity.

Compounds **6b**, **6d**, **6e**, **6g** and **6i** (Fig. 10) have demonstrated improved inhibitory activity compared to the drug standard acarbose. The binding landscape of each of these compounds is similar to one another. An extensive hydrophobic interaction system exists in each ligand–protein complex, along with hydrogen bond interactions and a

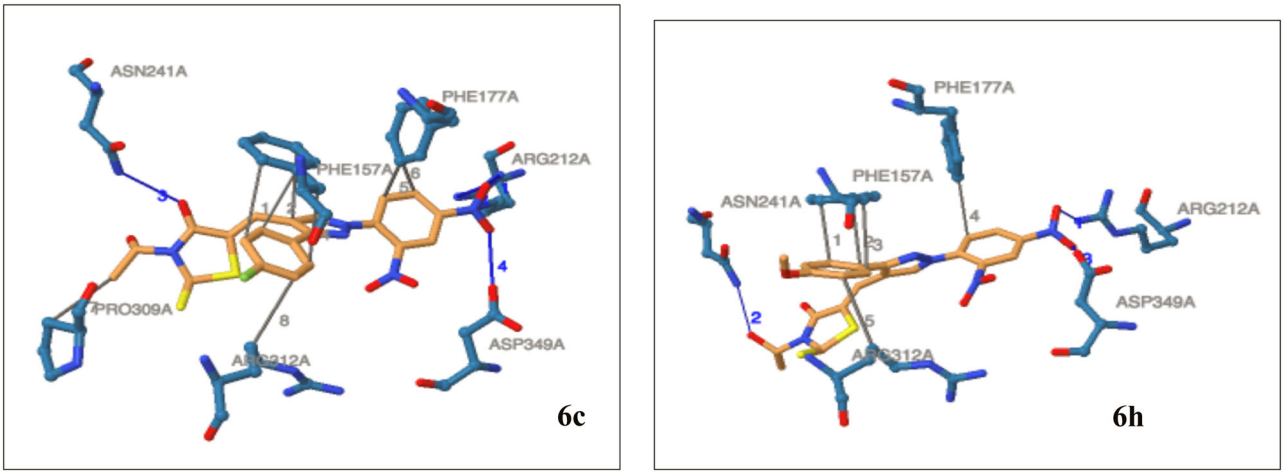

Fig. 11 2D representation of **6c** and **6h** in the binding pocket of α-glucosidase

distinct T-shaped π-stack. The binding structure of **6b** incorporated: hydrophobic interactions with residues Phe157, Arg312 and Tyr313 at a bond distance of 3.73/3.87/3.57, 3.70 and 3.85 Å, respectively; hydrogen bonds between Arg212 (amine group), Thr215 (hydroxyl group), Asn241 (amine group) and Asp349 (carboxyl group) with the ligands oxygen nitro groups (bond distance = 3.34/2.48, 2.23, 1.92 and 3.64 Å, respectively; bond angle = 113.4/116.2°, 129.8°, 166.7° and 110.7°, respectively); as well as a π-stack with amino acid Phe177 at 4.96 Å and angle of 71.76°. Compound **6d** has five hydrophobic interactions with Phe157, Phe300 and Arg312 at a bond distance of 3.32/3.76/3.80, 3.83 and 3.90 Å, respectively. The ligand acts as a hydrogen bond acceptor facilitating four distinct hydrogen bonds with Arg212 (amine group), Asn241 (amine group) and Asp349 (carboxyl group) (bond distance = 3.20/3.51, 2.12 and 3.19 Å, respectively; bond angle = 152.7/112.6°, 130.4° and 117.3°, respectively); as well as π-stacks with Phe177 at 4.81 Å and angle of 67.3°. The binding of **6e** in the binding pocket of α-glucosidase is stabilized by six hydrophobic interactions, six hydrogen bonds and a π-stack. The hydrophobic interactions involve residues Phe157, Pro309 and Arg312 (bond distance = 3.78/3.68/3.79, 3.80 and 3.37/3.79 Å, respectively) with a π-stacking with amino acid Phe177 (bond distance = 5.18 Å and bond angle = 77.08°). Hydrogens bonds originate from the proton donors Thr215 (side chain hydroxyl group), Asn241 (side chain amine), Glu276 (side chain carboxyl group), Arg312, Asp349 (side chain carboxyl group) and Arg439 (side chain amine) with the nitro group oxygen's of the ligand (bond distance = 2.37, 1.89, 3.17, 2.11, 3.16 and 3.49 Å, respectively; bond angle = 135.3°, 157.0°, 104.5°, 147.8°, 124.1° and 121.7°, respectively). The compound **6g** shares a π-stack with Phe177, bond distance of 4.82 Å and bond angle of 69.60°. Significant hydrogen bonding is exerted through donor residues Arg212 (amine group), Asn241 (amine group) and Asp (carboxyl group) at a bond distance of 3.17, 3.53 and 3.20 Å and bond angle of 153.0°, 117.9° and 115.0°, respectively. Residues Phe157, Pro309 and Arg312 contribute to the hydrophobic network at a distance of 3.30/3.19/3.65/3.88, 3.91 and 3.84 Å, respectively. In addition, compound **6i** has a unique binding profile driven by a distinct electrostatic interaction with chloride of the ligand and the carboxyl group of Asp408 at distance 3.71 Å, donor angle = 137.3° and

Table 3 Binding interactions of **6c** and **6h**

Compound	Residue identifier	Interaction type	Bond distance (Å)	Bond angle
6c	Phe157	Hydrophobic	3.69, 3.23, 3.79, 3.90	–
	Phe177	Hydrophobic	3.49, 3.87	–
	Pro309	Hydrophobic	3.85	–
	Arg312	Hydrophobic	3.71	–
	Arg212	Hydrogen bond	3.22, 2.65	113.6°, 141.3°
	Asn241	Hydrogen bond	2.40	119.6°
	Asp349	Hydrogen bond	2.98	123.7°
6h	Phe157	Hydrophobic	3.22, 3.49, 3.68	–
	Phe177	Hydrophobic	3.61	–
	Arg312	Hydrophobic	3.85	–
	Arg212	Hydrogen bond	2.40	121.4°
	Asn241	Hydrogen bond	2.37	118.4°
	Asp349	Hydrogen bond	2.52	132.3°

acceptor angle = 104.1°. Hydrophobic interactions with Phe157, Phe177 and Pro309 stabilize the ligand–protein complex (bond distance = 3.65/3.21/3.84/3.65/3.96, 3.50/3.87 and 3.87, respectively). Hydrogen bonds between Arg212, Asn241 and Asp349 enhance the selective binding profile of **6i** (bond distance = 3.23/2.73, 2.45 and 3.05 Å, respectively; bond angle = 135.5/142.3°, 118.0° and 121.4°, respectively).

Compounds **6c** and **6h** have the least inhibitory activity against α-glucosidase. The binding landscape of both ligands lacks the presence of a π-stack (Fig. 11). Table 3 summarizes the highlights of the integral residue interactions between the active site and ligand.

Conclusions

Two series of rhodanine containing compounds were successfully synthesized using the MH approach. Pyrazole–rhodanine conjugates (**6a–i**) exhibited superior α-glucosidase inhibitory activity to their simple rhodanine analogues (**8a–e**). The most potent conjugate **6f** ($IC_{50} = 2.259 \times 10^{-6}$ mol/L) displayed 42-fold better than that of acarbose. Interestingly, the unsubstituted derivative **6a** ($IC_{50} = 2.854 \times 10^{-5}$ mol/L) showed the second highest α-glucosidase inhibitory activity, which is also 3-fold better than that of acarbose. On the other hand, only two derivatives, **6d** ($IC_{50} = 6.377 \times 10^{-5}$ mol/L) and **6h** ($IC_{50} = 1.325 \times 10^{-4}$ mol/L) displayed strong inhibitory potential against α-amylase when compared to the standard inhibitor. Molecular docking studies further revealed three essential pharmacophoric features that are critical to exert α-glucosidase inhibition. This includes the nitro substituents on the phenyl ring; the hydrophobic bulk introduced by the pyrazole and conjugated ring structures, and; the 2-position of the unsubstituted phenyl ring (**6a**), in which the introduction of a strongly activating electron donating substituent (**6f**) at this position has been noted to improve inhibitory activity. Thus, only an electron donating substitution at position 2 would be tolerated to maintain or improve the drug candidate's antidiabetic activity.

Acknowledgements The authors would like to acknowledge the support from the NRF South Africa (Grant UID: 99563) as well as the CHPC in Cape Town for access to computational resources.

Compliance with ethical standards

Conflict of interest The authors declare that they have no conflict of interest.

References

Ademiluyi AO, Oboh G (2013) Soybean phenolic-rich extracts inhibit key-enzymes linked to type 2 diabetes (α-amylase and α-glucosidase) and hypertension (angiotensin I converting enzyme) in vitro. Exp Toxicol Pathol 65:305–309

Agrawal YP, Agrawal MY, Gupta AK (2015) Design, synthesis and evaluation of rhodanine derivatives as aldose reductase inhibitors. Chem Biol Drug Des 85:172–180

Andleeb H, Tehseen Y, Shah SJA, Khan I, Iqbal J, Hameed S (2016) Identification of novel pyrazole–rhodanine hybrid scaffolds as potent inhibitors of aldose reductase: design, synthesis, biological evaluation and molecular docking analysis. RSC Adv 6:77688–77700

Bathini P, Kameshwari L, Vijaya N (2013) Antidiabetic effect of 2 nitro benzimidazole in alloxan induced diabetic rats. Int J Basic Clin Pharma 2:814–818

Berube G (2016) An overview of molecular hybrids in drug discovery. Expert Opin Drug Discov 11:281–305

Browlee M (2001) Biochemistry and molecular cell biology of diabetic complications. Nature 14:813–820

Case DA, Babin V, Berryman J, Betz RM, Cai Q, Cerutti DS, Cheatham III TE, Darden TA, Duke RE, Gohlke H, Goetz AW, Gusarov S, Homeyer N, Janowski P, Kaus J, Kolossvary I, Kovalenko A, Lee TS, LeGrand S, Luchko T, Luo R, Madej B, Merz KM, Paesani F, Roe DR, Roitberg A, Sagui C, Salomon-Ferrer R, Seabra G, Simmerling CL, Smith W, Swails J, Walker RC, Wang J, Wolf RM, Wu X, Kollman PA (2014) AMBER 14. University of California, San Francisco, p 29–31

Chaudhry F, Naureen S, Choudhry S, Huma R, Ashraf M, Al-Rashida M, Jahan B, Khan MH, Iqbal F, Munawar MA, Khan MA (2018) Evaluation of α-glucosidase inhibiting potentials with docking calculations of synthesized arylidene-pyrazolones. Bioorg Chem 77:507–514

Guerreiro LR, Carreiro EP, Fernandes L, Cardote TAF, Moreira R, Caldeira AT, Guedes RC, Burke AJ (2013) Five-membered iminocyclitol α-glucosidase inhibitors: synthetic, biological screening and in silico studies. Biorg Med Chem 21:1911–1917

Hall BS, Bot C, Wilkinson SR (2011) Nifurtimox activation by trypanosomal type I nitroreductases generates cytotoxic nitrile metabolites. J Biol Chem 286:13088–13095

Hall BS, Wilkinson SR (2012) Activation of benznidazole by trypanosomal type I nitroreductases results in glyoxal formation. Antimicrob Agents Chemother 5:115–123

Ju KS, Parales RE (2010) Nitroaromatic compounds, from synthesis to biodegradation. Microbiol Mol Biol Rev 74:250–272

Kaku K (2014) Efficacy of voglibose in type-2 diabetes. Expert Opin Pharmacother 15:1181–1190

Kashtoh H, Muhammad MT, Khan JJ, Rasheed S, Khan A, Perveen S, Javaid K, Atia-tul W, Khan KM, Choudhary MI (2016) Dihydropyrano [2,3-c] pyrazole: novel in vitro inhibitors of yeast α-glucosidase. Bioorg Chem 65:61–72

Kazeem MI, Adamson JO, Ogunwande IA (2013) Modes of inhibition of α-amylase and α-glucosidase by aqueous extract of *Morinda lucida* Benth Leaf. BioMed Res Int 2013:527570

Kerru N, Bhaskaruni SVHS, Maddila S, Singh P, Jonnalagadda SB (2017a) Synthesis and antioxidant evaluation of a new class of thienopyrimidine–rhodanine hybrids. Lett Drug Des Discov 15:118–126

Kerru N, Singh P, Koorbanally N, Raj R, Kumar V (2017b) Recent advances (2015–2016) in anticancer hybrids. Eur J Med Chem 142:179–212

Khan KM, Rahim F, Wadood A, Kosar N, Taha M, Lalani S, Khan A, Fakhri MI, Junaid M, Rehman W (2014) Synthesis and molecular docking studies of potent α-glucosidase inhibitors based on biscoumarin skeleton. Eur J Med Chem 81:245–252

Kumar BRP, Nanjan MJ (2010) Novel glitazones: design, synthesis, glucose uptake and structure–activity relationships. Bioorg Med Chem Lett 20:1953–1956

Lovell SC, Davis IW, Arendall 3rd WB, de-Bakker PI, Word JM, Prisant MG, Richardson JS, Richardson DC (2003) Structure validation by Calpha geometry: phi, psi and Cbeta deviation. Proteins 50:437–450

Mandal SP, Mithuna, Garg A, Sahetya SS, Nagendra SR, Sripad HS, Manjunath MM, Sitaram, Soni M, Baig RN, Kumar SV, Kumar BRP (2016) Novel rhodanines with anticancer activity: design, synthesis and CoMSIA study. RSC Adv 6:58641–58653

Mata R, Cristians S, Rivera SE, Reyes KJ, Cruz IR (2013) Mexican antidiabetic herbs: valuable sources of inhibitors of α-glucosidases. J Nat Prod 76:468–483

Mendoza K, Kamila S, Biehl ER (2014) Synthesis of novel 5-aryl/hetarylidenyl 3-(2-methyl-5,6,7,8-tetrahydrobenzo[4,5]thieno[2,3-d]pyrimidin-4-yl)-2-thioxothiazolidin-4-ones. Heterocycles 88:741–753

Moorthy NS, Ramos MJ, Fernandes PA (2012) Studies on α-glucosidase inhibitors development: magic molecules for the treatment of carbohydrate mediated diseases. Mini Rev Med Chem 12:713–720

Murugan R, Anbazhagan S, Narayanan SS (2009) Synthesis and in vivo antidiabetic activity of novel dispiropyrrolidines through [3+2] cycloaddition reactions with thiazolidinedione and rhodanine derivatives. Eur J Med Chem 44:3272–3279

Patterson S, Wyllie S (2014) Nitro drugs for the treatment of trypanosomatid diseases: past, present, and future prospects. Trends Parasitol 30:289–298

Pettersen EF, Goddard TD, Huang CC, Couch GS, Greenblatt DM, Meng EC, Ferrin TE (2004) UCSF Chimera—a visualization system for exploratory research and analysis. J Comput Chem 25:1605–1612

Ramesh V, Rao BA, Sharma P, Swarna B, Thummuri D, Srinivas K, Naidu VGM, Rao VJ (2014) Synthesis and biological evaluation of new rhodanine analogues bearing 2-chloroquinoline and benzo[h]quinoline scaffolds as anticancer agents. Eur J Med Chem 83:569–580

Reddy TN, Ravinder M, Bagul P, Ravikanti K, Bagul C, Nanubolu JB, Srinivas K, Banerjee SK, Rao VJ (2014) Synthesis and biological evaluation of new epalrestat analogues as aldose reductase inhibitors (ARIs). Eur J Med Chem 71:53–66

Sales PM, Souza PM, Simeoni LA, Magalhaes PO, Silveira D (2012) α-Amylase inhibitors: a review of raw material and isolated compounds from plant source. J Pharm Pharm Sci 15:141–183

Sastry GM, Adzhigirey M, Day T, Annabhimoju R, Sherman W (2013) Protein and ligand preparation: parameters, protocols, and influence on virtual screening enrichments. J Comput Aided Mol Des 27:221–234

Shahidpour S, Panahi F, Yousefi R, Nourisefat M, Nabipoor M, Khalafi-Nezhad A (2015) Design and synthesis of new antidiabetic α-glucosidase and α-amylase inhibitors based on pyrimidine-fused heterocycles. Med Chem Res 24:3086–3096

Shai LJ, Masoko P, Mokgotho MP, Magano SP, Mogale AM, Boaduo N, Eloff JN (2010) Yeast alpha glucosidase inhibitory and antioxidant activities of six medicinal plants collected in Phalaborwa, South Africa. S Afr J Bot 76:465–470

Sharma SK, Panneerselvam A, Singh KP, Parmar G, Gadge P, Swami OC (2016) Teneligliptin in management of type 2 diabetes mellitus. Diabetes Metab Syndr Obes 9:251–260

Sievers F, Higgins DG (2014) Clustal Omega, accurate alignment of very large numbers of sequences. Methods Mol Biol 1079:105–116

Singh P, Jaiyeola B, Kerru N, Ebenezer O, Bissessur A (2017) A review of recent advancements in anti-tubercular molecular hybrids. Curr Med Chem 24:4180–4212

Singh P, Ngcoya N, Mopuri R, Kerru N, Manhas N, Ebenezer O, Islam MdS (2018) α-Glucosidase inhibition, antioxidant and docking studies of hydroxycoumarins and their mono and bis O-alkylated/acetylated analogs. Lett Drug Des Discov 15:127–135

Sundarram A, Murthy TPK (2014) α-Amylase production and applications: a review. J Appl Environ Microbiol 2:166–175

Taha M, Ismail NH, Javaid K, Imran S, Anouar EH, Wadood A, Atiatul W, Ali M, Khan KM, Saad SM, Rahim F, Choudhary MI (2015) Evaluation of 2-indolcarbohydrazones as potent α-glucosidase inhibitors, in silico studies and DFT based stereochemical predictions. Bioorg Chem 63:24–35

Taha M, Javid MT, Imran S, Selvaraj M, Chigurupati S, Ullah H, Rahim F, Mohammad JI, Khan KM (2017) Synthesis and study of the α-amylase inhibitory potential of thiadiazole quinoline derivatives. Bioorg Chem 74:179–186

Terashima H, Hama K, Yamamoto R, Tsuboshima M, Kikkawa R, Hatanaka I, Shigeta Y (1984) Effects of a new aldose reductase inhibitor on various tissues in vitro. J Pharmacol Exp Ther 229:226–230

Trott O, Olson AJ (2010) AutoDock Vina: improving the speed and accuracy of docking with a new scoring function, efficient optimization and multithreading. J Comput Chem 31:455–461

Vazquez EH, Ocampo-Montalban H, Ceron-Romero L, Cruz M, Gomez-Zamudio J, Hiriart-Valencia G, Villalobos-Molina R, Flores-Flores A, Estrada-Soto S (2017) Antidiabetic, antidyslipidemic and toxicity profile of ENV-2: a potent pyrazole derivative against diabetes and related diseases. Eur J Pharmacol 803:159–166

Viseras MEL, Fernandez B, Hilfiker S, Gonzalez CS, Gonzalez JL, Calahorro AJ, Colacio E, Rodriguez-Dieguez A (2014) In vivo potential antidiabetic activity of a novel zinc coordination compound based on 3-carboxy-pyrazole. J Inorg Biochem 131:64–67

Webb B, Sali A (2014) Protein structure modeling with MODELLER. Methods Mol Biol 1137:1–15

Werner MM, Patel BA, Talele TT, Ashby CR, Li Z, Zauhar RJ (2015) Dual inhibition of *Staphylococcus aureus* DNA gyrase and topoisomerase IV activity by phenylalanine-derived (Z)-5-arylmethylidene rhodanines. Bioorg Med Chem 23:6125–6137

Wiederstein M, Sippl MJ (2007) ProSA-web: interactive web service for the recognition of errors in three-dimensional structures of proteins. Nucleic Acids Res 35:W407–W410